NUCLEAR SCIENCE AND ENGINEERING · VOLUME 195 · 679–693 · JULY 2021

DOI: https://doi.org/10.1080/00295639.2021.1877989

Neutron Transmission and Capture Measurements of ^{133}Cs from 600 to 2000 eV

R. C. Block,[a]* J. A. Burke,[b] D. P. Barry,[b] M. J. Rapp,[b] S. Singh,[a] and Y. Danon[a]

[a]*Rensselaer Polytechnic Institute, Gaerttner LINAC Center, 110 8th Street, Troy, New York 12180*
[b]*Naval Nuclear Laboratory, P.O. Box 1072, Schenectady, New York 12301-1072*

Received March 12, 2020
Accepted for Publication January 15, 2021

Abstract — *Neutron capture and transmission measurements were carried out from thermal to 2000 eV on both solid and liquid samples containing elemental cesium (^{133}Cs). This work describes the extension of the R-matrix analysis of these data from 600 to 2000 eV by correcting the capture data for false capture in the NaI detector. These false capture–corrected capture and transmission data were analyzed for resonance parameters utilizing the SAMMY Bayesian analysis code to simultaneously fit both the capture and transmission data. Parameters were obtained for 53 cesium resonances over the 600- to 2000-eV energy range. The s-wave strength function was determined over the energy range from 0 to 1800 eV for both spin J = 3 and J = 4 resonances.*

Keywords — *Cesium, resonance parameters, neutron transmission, neutron capture yield, false capture correction.*

Note — *Some figures may be in color only in the electronic version.*

I. INTRODUCTION

The isotope ^{133}Cs is abundantly produced in nuclear reactors. About 7% of all fissions produce ^{133}Cs. Since neutrons inside a reactor interact with this large amount of material, it is important to have accurate cesium neutron cross-section data to perform the calculations necessary for the safe and efficient operation of reactors. To obtain these data, neutron capture and transmission measurements were carried out on Cs over the energy range from thermal to 2000 eV (Ref. 1). Previously, only the energy region from 0.01 to 600 eV had been analyzed for resonance parameters because the capture data were contaminated with false capture events above this energy range. This false capture is the result of neutrons scattered by the capture sample penetrating the $^{10}B_4C$ liner of the capture detector and subsequently being captured in the NaI of this detector. The capture data from 600 to 2000 eV have now been corrected for false capture, and the transmission and corrected capture data have been analyzed for resonance parameters over this energy region.

II. EXPERIMENTAL CONDITIONS

II.A. Overview of Measurements

The experimental conditions are described in our earlier Cs publication[1] and will be only briefly described here. Transmission and capture measurements were carried out using the time-of-flight (TOF) method with both liquid [cesium carbonate (Cs_2CO_3) dissolved in heavy water (D_2O)] and solid [cesium fluoride (CsF) crystals] samples containing cesium. The experimental details used for data acquisition are listed in Table I. The Rensselaer Polytechnic Institute Gaerttner LINAC Center linear accelerator was used to produce energetic electrons, and these electrons, in turn, impinged on water-cooled Ta plates to produce neutrons via the photoneutron reaction. The transmission measurements utilized a 1.27-cm-thick

*E-mail: blockr@rpi.edu

TABLE I

Experimental Details Showing Accelerator and Data Acquisition Parameters

Measurement (Cs Sample)	Overlap Filter (Thickness)	Neutron Target	Electron Pulse Width (μs)	Average Electron Current (μA)	Electron Energy (MeV)	Neutron Energy Region (eV)	Channel Width (μs)	Repetition Rate (pps)	Flight Path (m)
Transmission (liquid)	B_4C (7.9 mm)	Bare bounce	0.100	26	54	$E < 4.0$ $4.0 < E < 45$ $45 < E < 262$ $262 < E$	8 0.50 0.0625 0.03125	225	25.596 ± 0.006
Transmission (crystal)	B_4C (7.9 mm)	Bare bounce	0.050	19	62	$E < 16$ $16 < E < 84$ $84 < E < 372$ $372 < E$	4 0.25 0.0625 0.03125	250	26.868 ± 0.003
Capture (liquid)	B_4C (7.9 mm)	Bare bounce	0.056	13	67	$E < 15$ $15 < E < 76$ $76 < E < 312$ $312 < E$	4 0.25 0.0625 0.03125	250	25.564 ± 0.006
Capture (crystal)	B_4C (7.9 mm)	Bare bounce	0.056	16	64	$E < 15$ $15 < E < 76$ $76 < E < 333$ $333 < E$	4 0.25 0.0625 0.03125	250	25.564 ± 0.006

(0.5-in.-thick) ^{6}Li glass detector at the 25-m flight station with the glass viewed by two photomultipliers located outside of the neutron beam.[2] The capture measurements utilized the 16-section NaI multiplicity detector also located at the 25-m flight station.[3] This detector is illustrated in Fig. 1, where a neutron beam is incident upon a capture sample placed in the middle of the detector. The capture sample is surrounded by the 16 NaI pie-shaped crystals that detect capture gamma rays. Neutron capture is defined as an event when the sum of energy deposited in all 16 sections exceeds a discriminator (bias) level of 1 MeV; multiplicity is defined as the number of sections that have an energy deposit that exceeds 100 keV.

The neutron intensity from the accelerator was monitored with moderated fission chambers located at an ≈9-m flight path; a ^{6}Li glass ring detector placed in the epithermal transmission flight tube; and when applicable, a ^{6}Li glass detector located at the 15-m flight path. These monitor detectors were used to minimize the effects of beam intensity fluctuations as well as correct for different collection times for the various sample in and out positions.

II.B. Sample Information

Two types of samples were used for these measurements: a set of CsF crystals and a set of liquid samples consisting of Cs_2CO_3 dissolved in D_2O. The CsF crystals provided thick samples while the liquid samples provided thin samples of uniform thickness. The CsF crystals were encapsulated in 0.51-mm-thick aluminum cans with 76.2-μm-thick Mylar films between the crystals and aluminum. The liquid samples were prepared by dissolving Cs_2CO_3 powder into D_2O and sealing the solution into cylindrical quartz cells with windows with 3.81-cm inside diameter and 0.159-cm thickness.

II.B.1. CsF Samples

Three thicknesses of CsF were used for these measurements with nominal thicknesses of 6.86, 20.1, and 25.2 mm. The samples were not rigid solids but were rather somewhat jelly-like in consistency. However, they did have two well-defined parallel faces. The sample thicknesses were determined by measuring the outer thickness of the CsF-Mylar-aluminum assembly and subtracting the 1.02-mm aluminum and 0.15-mm Mylar thicknesses. The CsF thickness uncertainty is estimated as ±0.25 mm. Table II lists the atomic number densities of the Cs and F in the crystals and the C, O, and H in the two 0.076-mm-thick films of Mylar. Errors in sample thickness are 1σ errors.

II.B.2. Liquid Samples

Cesium carbonate powder was dissolved into D_2O to produce a stock solution, and portions of this stock solution were further diluted with D_2O to produce the three cesium liquid samples. Chemical analysis of the powder indicated that it was a mixture of 93.1% Cs_2CO_3 and 6.9% cesium bicarbonate. This powder also contained 1% water (by weight). In addition to the Cs samples, two D_2O-filled quartz cylinders were utilized to provide samples with the same thickness of D_2O as the thickness of the Cs liquid samples. Table III lists the thickness of the liquids in each cell and the atomic number densities of

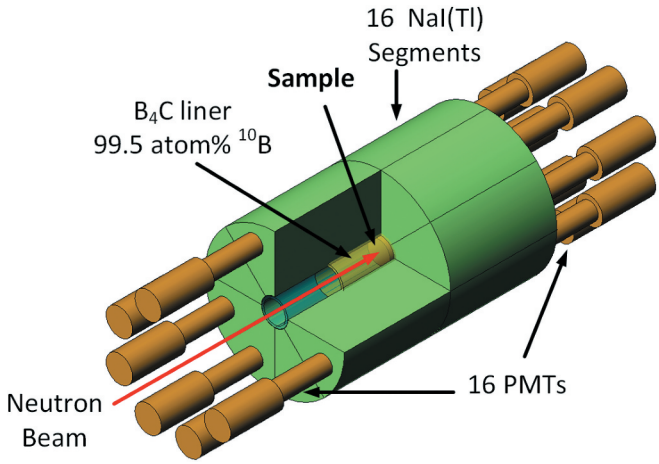

Fig. 1. The capture gamma-ray multiplicity detector. A neutron beam is shown incident upon a sample placed at the center of the detector. Capture gamma rays are detected in the 16 optically isolated NaI segments. The B_4C liner is designed to minimize neutrons scattered by the sample from penetrating to the NaI detectors. (This figure was obtained from Ref. 4.)

TABLE II

The Atomic Number Densities of the CsF Samples and Mylar Films

Nominal Thickness (mm)	N_{Cs} (atom/b)	N_F (atom/b)	N_C (atom/b)	N_O (atom/b)	N_H (atom/b)
6.86	$(1.032 \pm 0.060) \times 10^{-2}$	$(1.032 \pm 0.060) \times 10^{-2}$	$(6.86 \pm 1.14) \times 10^{-4}$	$(2.74 \pm 0.46) \times 10^{-4}$	$(5.49 \pm 0.91) \times 10^{-4}$
20.1	$(3.182 \pm 0.063) \times 10^{-2}$	$(3.182 \pm 0.063) \times 10^{-2}$	$(6.86 \pm 1.14) \times 10^{-4}$	$(2.74 \pm 0.46) \times 10^{-4}$	$(5.49 \pm 0.91) \times 10^{-4}$
25.2	$(4.057 \pm 0.064) \times 10^{-2}$	$(4.057 \pm 0.064) \times 10^{-2}$	$(6.86 \pm 1.14) \times 10^{-4}$	$(2.74 \pm 0.46) \times 10^{-4}$	$(5.49 \pm 0.91) \times 10^{-4}$

TABLE III

The Liquid Thickness and Atomic Number Densities of the Cesium Solution and D_2O-Filled Cells

Cell Number	Thickness (mm)	N_{Cs} (atom/b)	N_C (atom/b)	N_O (atom/b)	N_H (atom/b)	N_D (atom/b)
L-4	3.18	$(2.53 \pm 0.06) \times 10^{-4}$	$(1.68 \pm 0.04) \times 10^{-4}$	$(1.09 \pm 0.03) \times 10^{-2}$	$(1.33 \pm 0.03) \times 10^{-4}$	$(2.08 \pm 0.05) \times 10^{-2}$
L-5	3.18	$(8.71 \pm 0.02) \times 10^{-4}$	$(5.80 \pm 0.14) \times 10^{-4}$	$(1.08 \pm 0.03) \times 10^{-2}$	$(4.59 \pm 0.11) \times 10^{-4}$	$(1.80 \pm 0.04) \times 10^{-2}$
L-7	6.35	$(2.96 \pm 0.06) \times 10^{-3}$	$(1.97 \pm 0.04) \times 10^{-3}$	$(2.08 \pm 0.04) \times 10^{-2}$	$(1.56 \pm 0.03) \times 10^{-3}$	$(2.92 \pm 0.06) \times 10^{-2}$
L-6	3.18			$(1.07 \pm 0.03) \times 10^{-2}$		$(2.14 \pm 0.05) \times 10^{-2}$
L-8	6.35			$(2.11 \pm 0.04) \times 10^{-2}$		$(4.21 \pm 0.09) \times 10^{-2}$

the Cs, C, O, H, and D in these cells (including the 1% water).

The quartz cells had a wall thickness of 1.59 mm. For these measurements the neutron beam impinged perpendicularly on the face of the cylindrically shaped samples.

III. DATA REDUCTION

III.A. Neutron Energy

In the nonrelativistic approximation, the incident neutron energy (in units of electron volt) measured at TOF channel i is

$$E_i = \left[\frac{72.29824L}{t_i - t_0}\right]^2 , \quad (1)$$

where

E_i = energy (eV)

L = flight path (m)

$(t_i - t_0)$ = neutron TOF (μs).

The recorded time of an event in channel i is t_i while t_0 is the time when the electron pulse strikes the neutron target. By measuring the time when the gamma flash is detected, t_0 is obtained by correcting for the flight time of these gamma rays from the neutron target to the detector.

III.B. Capture Yield

The experimental capture yield $Y_{\gamma exp,i}$ in TOF channel i is

$$Y_{\gamma exp,i} = \frac{Capture\ \ Rate}{Incident\ \ Neutron\ \ Rate} = \frac{\frac{C_i - B_i}{\eta_c}}{f\varphi_{r,i}} = \frac{C_i - B_i}{K\varphi_{r,i}} , \quad (2)$$

where the numerator refers to the net capture rate with the capture sample in the beam and the denominator to the neutron rate incident upon the capture sample and

C_i = dead-time–corrected and beam-monitor–normalized counting rate with the capture sample in the beam

B_i = background counting rate with either the equal-thickness D_2O sample or empty aluminum can in the beam

η_c = constant that is the capture detector efficiency and converts the capture counting rate to the capture rate.

The relative neutron flux incident upon the capture sample $\varphi_{r,i}$ was determined from a measurement with a $^{10}B_4C$ sample placed in the neutron beam inside the multiplicity detector. These neutron counting data were dead time corrected and background subtracted. The relative neutron flux is equal to the resulting net counting data divided by the efficiency for detecting the gamma ray from the $^{10}B(n;\alpha,\gamma)$ reaction. The constant f normalizes the relative flux to the actual neutron flux incident upon the capture sample. The normalization constant K is equal to the product $\eta_c f$.

The normalization constant K is typically determined by measuring capture in a region where the capture yield Y_γ is known, typically near a saturated resonance that is mostly the result of neutron capture. The liquid sample and CsF capture yields were normalized to the saturated capture level at the energy of 22.5 eV.

III.C. Correction for False Capture

A simplified sketch of the capture multiplicity detector[3] is shown in Fig. 2, where a neutron (dashed horizontal line) is scattered by the capture sample (dashed slanted line), passes through the $^{10}B_4C$ liner, and is subsequently captured in the NaI of this detector with the production of capture gamma rays (dotted curved lines). This capture in NaI is called false capture, and it occurs at some time after the neutron scatters from the sample.

False capture is calculated by transporting the scattered neutrons into the multiplicity detector and determining how many are subsequently captured in the NaI (mostly in iodine). This is done in the following four steps for neutrons with TOF t_i incident upon the sample:

1. Measure the number of false capture counts in channel i by placing a pure scattering sample into the detector and dividing these counts by the detector efficiency to obtain the number of false captures in channel i. These false captures per channel are then divided by the number of scattered neutrons in channel i. This will be called $FCSN_i$, the false capture per scattered neutron at TOF t_i.

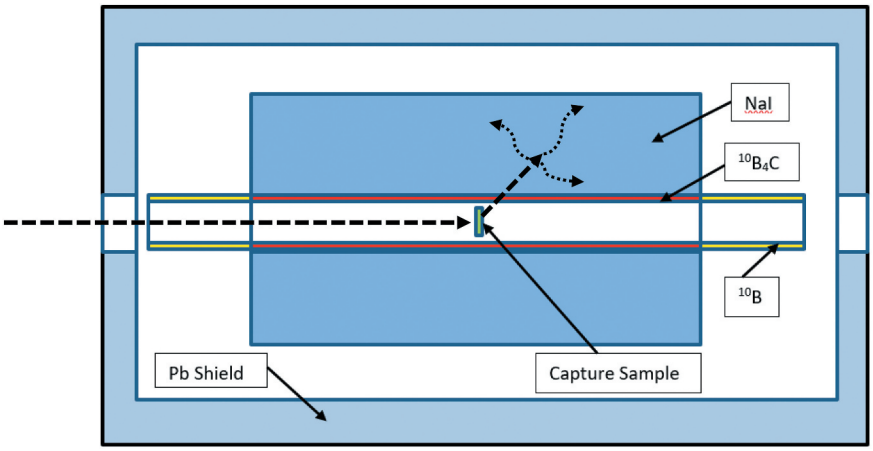

Fig. 2. Sketch of the NaI multiplicity detector. The $^{10}B_4C$ liner is 1 cm thick enriched to 99.46% in ^{10}B. A neutron (dashed horizontal line) strikes the capture sample, is scattered by the capture sample, passes through the $^{10}B_4C$ liner into the NaI (dashed slanted line), and is captured in the NaI to produce false capture gamma rays (dotted curved lines).

2. Calculate the neutron yield $Y_{n,i}$, which is the number of neutrons scattered per neutron incident on the sample at t_i.

3. Multiply $Y_{n,i}$ by $FCSN_i$ to obtain the total amount of false capture produced by neutrons scattered at t_i. This will be called the total false capture yield $Y_{FCtot,i}$.

4. It takes time for the neutrons scattered by the sample to be transported into the detector and subsequently be captured. To account for this time, distribute $Y_{FCtot,i}$ over times following the time at which the neutron strikes the sample.

The ratio of false capture to capture in an isolated resonance is a useful measure of the importance of false capture in a resonance. An approximate value of this ratio is derived in the Appendix.

III.C.1. Number of False Captures per Scattered Neutron FCSN$_i$

The number of false captures per scattered neutron $FCSN_i$ is determined by placing a pure scattering sample into the multiplicity capture detector and observing the false capture counts. For a measurement over the 600- to 2000-eV energy range, a lead sample provides an almost pure scattering sample with no resonance structure. Figure 3 shows the measured total number of false capture counts per scattered neutron (labeled "f_c" in Fig. 3) by a sample of lead in the multiplicity detector.[4] Note that this function varies smoothly over this energy range and that it is only near 3 keV where the influence of the Na resonance in the NaI crystals exhibits any significant resonance structure.

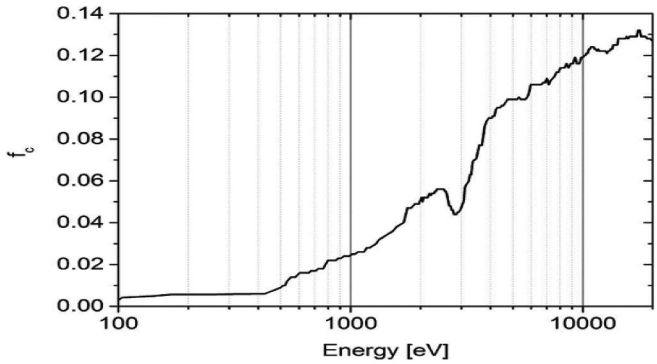

Fig. 3. The false capture counts per scattered neutron f_c for neutrons scattered by a 2.72-mm-thick sample of lead with a 2-MeV detector total deposited energy discrimination. These data were obtained by smoothing the incident neutron spectrum.

The false capture counts per scattered neutron data in Fig. 3 were measured with a detector bias of 2 MeV. Therefore, the total number of false captures per neutron scattered at energy E, $FCSN(E)$, is equal to f_c divided by the detection efficiency for false capture at a 2-MeV detector total deposited energy discrimination.

III.C.2. Number of Scattered Neutrons per Incident Neutron: Y$_n$

For a beam of monoenergetic neutrons incident upon a uniform thickness sample, such as shown in Fig. 2, the total number of interactions per incident neutron is equal to $(1 - T)$, where T is the transmission through the

sample. For nonfissile nuclei the number of scatters per incident neutron is equal to

$$No.\ scatters\ per\ incident\ neutron = Y_n = (1 - T) - Y_\gamma \quad , \tag{3}$$

where Y_n is the neutron yield (scatters per incident neutron) and Y_γ is the capture yield (captures per incident neutron).

The neutron yield Y_n can be calculated from the sample's resonance parameters and experimental conditions (such as resolution broadening, sample temperature, etc.). For this Cs analysis the Bayesian code SAMMY (Ref. 5) was used to calculate the transmission and capture yield.

III.C.3. Time-Distributed False Capture per Scattered Neutron

The total number of false captures per incident neutron with energy E, $Y_{FCtot}(E)$, is distributed over times from when the neutron strikes the sample until the last false capture event occurs. This time-distributed false capture was calculated using the MCNP-PoliMi Monte Carlo code[6] with a CsF sample.

For TOF experiments such as this measurement, data are taken in sequential TOF intervals with each interval designated as a channel. At TOF channel i the time-distributed false capture from all preceding channels is summed to provide the total time-distributed false capture yield in channel i. This is designated as $Y_{FCdist,i}$. To correct the experimental capture yield data in channel i, $Y_{\gamma exp,i}$, for false capture, the following is applied:

$$Y_{\gamma,i} = Y_{\gamma exp,i} - Y_{FCdist,i} \quad , \tag{4}$$

where $Y_{\gamma,i}$ is the false capture–corrected capture yield. It is this yield that is used in the SAMMY analysis.

III.D. Transmission

Transmission is defined as the ratio of the detector counting rate with a sample in the beam to the counting rate with the sample out of the beam. The neutron transmission T_i in TOF channel i is given by

$$T_i = \frac{C_i^S - K_S B_i - B_S}{C_i^O - K_O B_i - B_O} \quad , \tag{5}$$

where

$C_i^S,\ C_i^O$ = dead-time–corrected and monitor-normalized counting rates for the sample and open measurements, respectively

B_i = unnormalized time-dependent background counting rate

B_S, B_O = steady-state background counting rates for the sample and open measurements, respectively

$K_S,\ K_O$ = background normalization factors for the sample and open measurements, respectively.

(Note that the open sample refers to either the equal-thickness D_2O sample for the liquid sample or the empty aluminum container for the CsF sample measurements.)

The determination of the time-dependent background is one of the more difficult tasks to accomplish. This background was determined by cycling into the beam a set of samples, called notches, containing blacked-out resonances and then extrapolating to the sample and open conditions without the notch samples in the beam. For these transmission measurements, a 0.635-cm-thick metallic Na sample was placed in the beam to provide a permanent notch near a neutron energy of 2.8 keV. The 2.8-keV notch lies well above the 2-keV upper limit for the data analyzed in this paper. Samples of Ag, W, and Co were cycled in the beam during the notch measurements with liquid samples to produce notches near 5.2, 18.6, and 132 eV, respectively. The shape of the background, in TOF, is determined with all these notches in the beam; this shape is then normalized to the 2.8-keV notch present in all the open and transmission sample measurements.

For the CsF samples the transmission is that of the CsF and two sheets of 0.15-mm-thick Mylar. For the liquid samples the transmission is that of the Cs-containing-liquid sample counting rate divided by the corresponding D_2O compensator sample counting rate.

IV. RESULTS

The transmission and capture data were analyzed for resonance parameters using the R-matrix Bayesian code SAMMY version 8 (Ref. 5). The analysis employed the experimental resolution, Doppler broadening, self-shielding, multiple scattering, and Reich-Moore approximation features of SAMMY. This code takes into account the statistical fluctuations in the experimental data points and known uncertainties in experimental parameters such as sample thickness, detector efficiency, flight path length, etc. Both the transmission and capture yield data were fitted, and a final set of resonance

parameters was obtained for the best overall fit to all of the data. Both s-wave (l = 0) and p-wave (l = 1) resonances were observed in this experiment.

IV.A. Capture Yield and Transmission Plots

The capture yield and transmission data are plotted in Figs. 4 through 7. These plots show the capture and transmission data and the SAMMY fits to these data and to data derived from the ENDF/B-VIII.0 (Ref. 7) evaluated Cs resonance parameters. The plots show

1. the Cs capture yield, corrected for false capture, and transmission data plotted as solid colored circles, each color corresponding to a given sample
2. the SAMMY fits to the data plotted as solid colored lines with the colors corresponding to the samples
3. the ENDF evaluated yield and transmission plotted as dashed lines.

An overall view of these results is plotted in Figs. 4 and 5 for the energy ranges 600 to 1300 eV and 1300

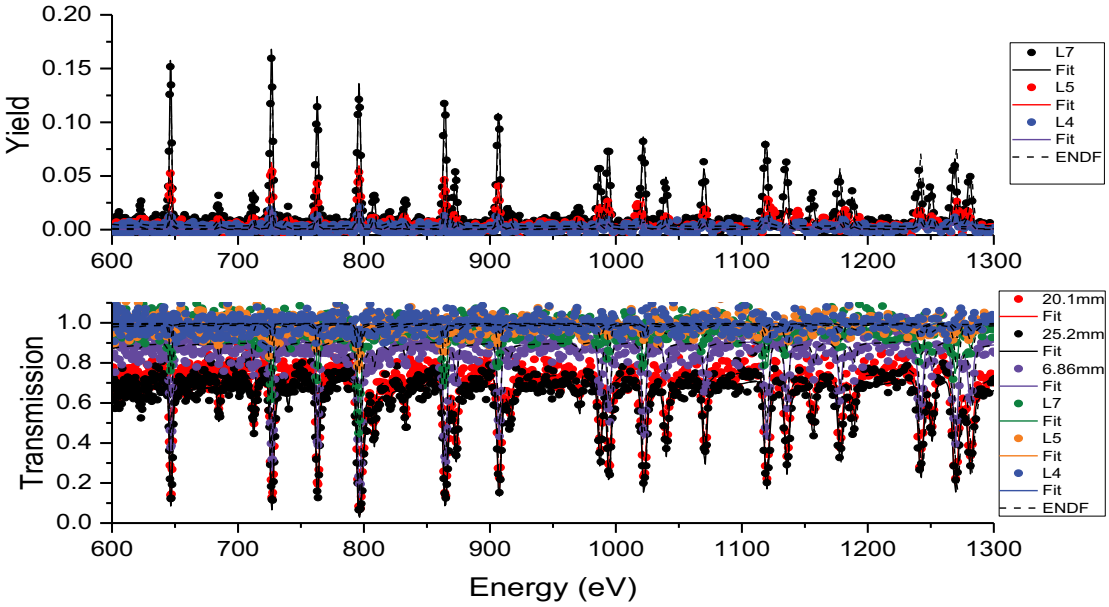

Fig. 4. Capture yield and transmission from 600 to 1300 eV for liquid and solid Cs samples. The labels 6.86 mm, 20.1 mm, and 25.2 mm refer to the CsF sample thicknesses. The ENDF labels refer to ENDF/B-VIII.0.

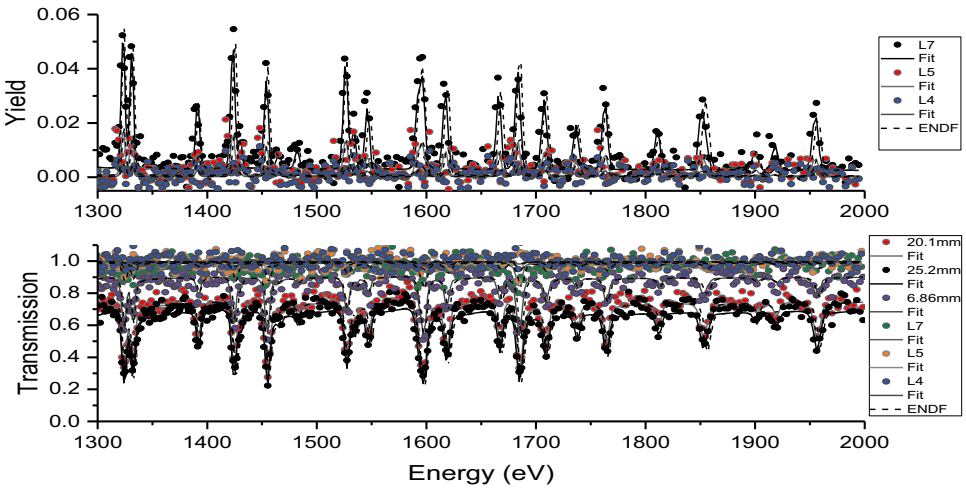

Fig. 5. Capture yield and transmission from 1300 to 2000 eV for liquid and solid Cs samples. The labels 6.86 mm, 20.1 mm, and 25.2 mm refer to the CsF sample thicknesses. The ENDF labels refer to ENDF/B-VIII.0.

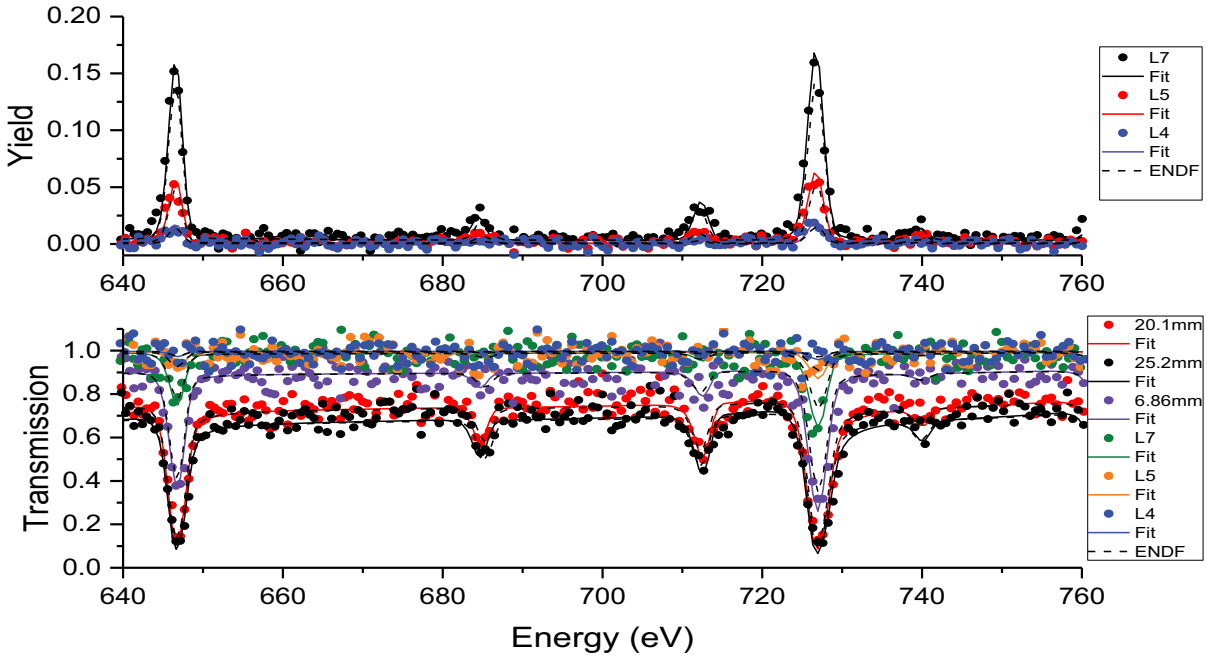

Fig. 6. Capture yield and transmission from 640 to 760 eV for liquid and solid Cs samples. The labels 6.86 mm, 20.1 mm, and 25.2 mm refer to the CsF sample thicknesses. The ENDF labels refer to ENDF/B-VIII.0.

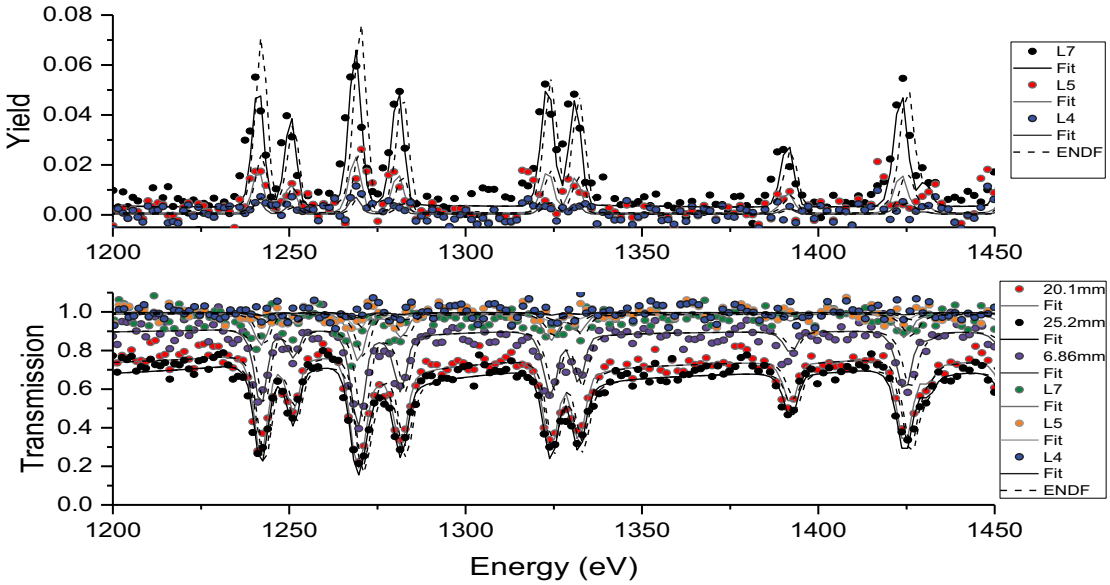

Fig. 7. Capture yield and transmission from 1200 to 1450 eV for liquid and solid Cs samples. The labels 6.86 mm, 20.1 mm, and 25.2 mm refer to the CsF sample thicknesses. The ENDF labels refer to ENDF/B-VIII.0.

to 2000 eV, respectively. The resonances appear to be well separated from each other and thus should provide a good estimate of the average level spacing. To illustrate a more detailed view of these results, Figs. 6 and 7 show a limited energy range of 640 to 760 eV and 1200 to 1450 eV, respectively.

IV.B. Resonance Parameters

Table IV lists the resonance parameters obtained from the analysis of these transmission and capture data. The SAMMY analyses of the measured yield and transmission data started with the ENDF/B-VIII.0

(Ref. 7) resonance parameters as input parameters. A major objective of these measurements is to determine the neutron and radiation width for each resonance. The neutron width can be obtained for all the resonances, but the radiation width can be obtained only from resonances that have a large amount of scattering. The criterion of $\Gamma_\gamma/\Gamma_n < 5$ was adopted from Barry[2] to reflect the sensitivity for determining the radiation width from a SAMMY analysis of the resonance data. For resonances with $\Gamma_\gamma/\Gamma_n > 5$, the radiation widths were initially set equal to the ENDF value of 120 meV to obtain preliminary values of the radiation widths. Finally, these ENDF starting values were replaced by the average radiation widths of 105 and 116 meV for spin 3 and 4 resonances, respectively.

In Table IV the SAMMY resonance energy E_o, radiation width Γ_γ, and neutron width Γ_n are listed in columns 1, 5, and 9, respectively. The corresponding ENDF resonance parameters $E_{o,endf}$, $\Gamma_{\gamma,endf}$, and $\Gamma_{n,endf}$ are listed in columns 4, 8, and 12, respectively. The SAMMY (Bayesian) absolute uncertainties in the resonance parameters $\Delta E_{o,B}$, $\Delta\Gamma_{\gamma,B}$, and $\Delta\Gamma_{n,B}$ are listed in columns 2, 6, and 10, respectively. The external uncertainties $\Delta E_{o,ext}$, $\Delta\Gamma_{\gamma,ext}$, and $\Delta\Gamma_{n,ext}$ are listed in columns 3, 7, and 11, respectively. Column 13 lists the total angular momentum J of the resonances, and column 14 lists the orbital angular momentum l. All uncertainties are 1σ.

As a check on the effect of false capture on the SAMMY analysis, a SAMMY calculation was done with the raw capture data, i.e., capture data not corrected for false capture. The false capture correction resulted in an average radiation width that was 10% smaller than that obtained without the correction. The average neutron width was 2.7% smaller with the false capture correction. Thus, for this experiment false capture correction affects the radiation widths more than the neutron widths.

External uncertainties are a measure of the fluctuations in the resonance parameters (E_o, Γ_γ, Γ_n) when each of the ten epithermal measurements is individually solved by SAMMY with the same input parameters (in this analysis the ENDF parameters were used as the common input parameters).

The external uncertainty in E_o, Γ_γ, or Γ_n is determined from the mean square deviation Eq. (6):

$$\Delta X_{ext} = \sqrt{\left\{\sum_1^n \frac{(X_i - \langle X\rangle)^2}{(\Delta X_{B,i})^2}\right\} \Big/ \left\{(n-1)\sum_1^n \frac{1}{(\Delta X_{B,i})^2}\right\}} \ , \tag{6}$$

where X stands for E_o, Γ_γ, or Γ_n, and n is the number of measurements (four capture and six transmission). The value $\Delta X_{B,i}$ in Eq. (6) is the Bayesian SAMMY uncertainty in E_o, Γ_γ, or Γ_n for each sample i.

The weighted-average parameter $<X>$ in Eq. (6) is determined from Eq. (7):

$$< X > = \sum_1^n \frac{X_i}{(\Delta X_{B,i})^2} \Big/ \sum_1^n \frac{1}{(\Delta X_{B,i})^2} \ . \tag{7}$$

It is recommended that the larger of these two errors, the Bayesian or the external error, be used in applying these results.

IV.C. Strength Function

The strength function is defined in Eq. (8) as the average reduced neutron width $< \Gamma_n^o >$ divided by the average level spacing $\langle D\rangle$:

$$SF \equiv < \Gamma_n^o > / \langle D\rangle \ . \tag{8}$$

The reduced neutron width Γ_n^o is equal to the neutron width Γ_n divided by the square root of the resonance energy E_o.

Using the method of Liou and Rainwater,[8] the average reduced neutron width is

$$< \Gamma_n^o > = \frac{1}{N}\sum_1^N \Gamma_{n,i}^o \ , \tag{9}$$

where N is the number of levels and the average level spacing is

$$< D > = (E_{max} - E_{min})/(N-1) \ , \tag{10}$$

where E_{max} and E_{min} are the energies of the highest- and lowest-energy resonances of the N levels, respectively.

To obtain the Cs strength function, we can combine the resonance parameters up to 600 eV (Ref. 1) with these data from 600 to 2000 eV. Figure 8 is a plot of the cumulative sum of positive energy Cs resonances up to 2000 eV. For a constant level spacing, the cumulative sum will be linear with energy. The cumulative sum in Fig. 8 is approximately linear until about 1800 eV; above this energy the sum appears to be "falling off" linearity, probably the result of missing levels. Thus, only data below 1800 eV will be used in determining the strength function.

TABLE IV

Resonance Parameters Obtained from the Measurements of 600 to 2000 eV*

E_o	$\Delta E_{o,B}$	$\Delta E_{o,ext}$	$E_{o,endf}$	Γ_γ	$\Delta\Gamma_{\gamma,B}$	$\Delta\Gamma_{\gamma,ext}$	$\Gamma_{\gamma,endf}$	Γ_n	$\Delta\Gamma_{n,B}$	$\Delta\Gamma_{n,ext}$	$\Gamma_{n,endf}$	J	l
646.51	0.01	0.020	685.0	142	8.9	1.0	120	67.0	1.9	0.7	56.89	4	0
684.37	0.02	0.003	685.0	116			120	5.5	0.4	0.1	5.511	4	0
712.43	0.04	0.14	712.00	116			59.0	9.9	0.3	0.36		4	1
726.63	0.02	0.012	726.7	134	6.3	1.4	120	140.9	3.7	2.3	96.00	4	0
739.70	0.17	0.028	739.5	116			120	3.1	0.2	0.0	3.111	4	0
762.89	0.02	0.024	762.9	133	8.6	2.7	120	117.0	3.4	2.1	76.57	3	0
796.08	0.02	0.019	796.1	120	2.8	0.3	120	402.5	5.5	7.1	348.4	4	0
807.86	0.07	0.010	807.8	116			120	12.7	0.6	0.1	11.56	4	0
832.61	0.09	0.024	832.5	116			120	10.1	0.6	0.1	7.467	4	0
864.17	0.02	0.020	864.2	144	4.7	0.2	106	264.1	6.1	5.6	236.6	3	0
872.52	0.02	0.001	872.9	125	12.1	0.3	120	35.4	1.6	0.3	36.80	3	0
906.79	0.03	0.024	906.9	168	9.2	0.4	134	151.2	5.0	0.8	120.0	3	0
915.75	0.12	0.034	916.2	105			120	12.2	0.8	0.1	12.00	3	0
970.57	0.15	0.021	970.5	116			120	9.4	0.6	0.1	8.711	4	0
986.75	0.02	0.007	987.2	128	12.0	0.4	120	67.8	2.8	1.5	51.43	3	0
993.91	0.03	0.007	994.3	127	10.3	1.5	120	117.4	4.4	2.5	89.14	3	0
1021.59	0.03	0.014	1022	90	4.7	2.0	108	178.2	6.0	2.9	151.1	4	0
1039.30	0.06	0.031	1039	130	11.8	0.1	120	51.7	2.3	0.3	44.57	3	0
1069.96	0.05	0.036	1070	144	11.5	0.5	120	76.5	3.1	0.6	59.43	3	0
1119.01	0.03	0.018	1119	118	6.3	1.7	128	195.6	6.6	4.1	156.4	4	0
1135.11	0.05	0.029	1135	113	8.1	2.0	120	124.8	5.7	2.1	133.7	3	0
1155.74	0.01	0.002	1157	119	11.9	0.4	120	28.4	1.7	0.5	28.44	4	0
1177.24	0.03	0.007	1178	108	10.1	2.1	120	74.9	3.5	1.6	76.89	4	0
1187.61	0.00	0.001	1189	118	11.9	0.2	120	27.9	1.8	0.5	26.67	4	0
1241.03	0.04	0.049	1242	70	5.2	2.2	120	181.1	7.5	2.9	183.1	4	0
1250.27	0.10	0.053	1251	131	12.2	1.2	120	43.9	2.6	0.6	40.89	4	0
1268.54	0.03	0.017	1270	95	4.6	1.5	121	324.8	9.4	4.3	291.6	4	0
1280.63	0.02	0.001	1282	98	8.5	0.1	93	168.5	8.1	1.7	173.1	3	0
1323.07	0.03	0.008	1324	114	9.7	3.5	131	214.2	9.4	3.5	184.0	3	0
1330.91	0.02	0.001	1332	107	9.8	0.2	107	143.9	7.8	2.9	164.6	3	0
1391.07	0.02	0.002	1392	118	11.8	0.4	120	54.9	3.5	1.2	46.86	3	0
1423.24	0.02	0.005	1425	93	8.4	2.4	104	175.2	8.5	1.9	167.1	4	0
1429.96	0.09	0.003	1430	121	12.0	0.1	120	17.1	1.5	0.2	14.86	3	0
1453.73	0.02	0.004	1455	74	7.4	1.7	94	297.1	12.2	8.8	244.6	3	0
1465.07	0.31	0.295	1463	105			120	10.7	1.0	0.1	11.09	3	0
1481.87	0.11	0.001	1483	120	12.0	0.0	120	13.0	1.3	0.2	14.29	3	0
1526.04	0.01	0.002	1527	119	11.6	1.4	126	120.2	6.8	2.0	114.7	4	0
1533.39	0.02	0.001	1536	124	12.2	0.4	120	34.2	2.8	0.5	31.43	3	0
1545.92	0.02	0.002	1548	116	11.8	0.3	120	46.4	3.3	0.7	44.44	4	0

(Continued)

TABLE IV (Continued)

E_o	$\Delta E_{o,B}$	$\Delta E_{o,ext}$	$E_{o,endf}$	Γ_γ	$\Delta\Gamma_{\gamma,B}$	$\Delta\Gamma_{\gamma,ext}$	$\Gamma_{\gamma,endf}$	Γ_n	$\Delta\Gamma_{n,B}$	$\Delta\Gamma_{n,ext}$	$\Gamma_{n,endf}$	J	1
1591.51	0.01	0.002	1593	120	12.0	0.1	120	43.8	3.1	0.7	38.22	4	0
1596.25	0.09	0.029	1597	99	6.3	1.4	101	381.9	16.4	10.8	408.00	3	0
1617.15	0.02	0.003	1619	105	10.7	1.7	120	135.5	8.8	3.3	165.71	3	0
1665.80	0.07	0.005	1668	113	11.3	0.9	120	83.9	5.7	0.8	90.67	4	0
1683.28	0.07	0.023	1685	93	8.1	2.3	121	348.0	17.1	3.2	359.11	4	0
1707.35	0.01	0.001	1709	115	11.4	0.7	120	134.9	9.0	1.5	146.29	3	0
1736.34	0.02	0.001	1738	120	12.0	0.1	120	41.7	3.4	0.2	43.56	4	0
1762.66	0.01	0.001	1764	116	11.5	0.7	120	134.9	9.0	0.8	139.43	3	0
1810.65	0.02	0.000	1812	121	12.1	0.1	120	36.4	3.1	0.2	36.44	4	0
1850.60	0.01	0.001	1854	120	11.9	0.1	120	63.4	5.3	0.7	65.78	4	0
1854.79	0.61	0.030	1857	119	11.9	0.0	120	30.3	2.7	0.1	30.86	3	0
1899.90	0.04	0.001	1901	121	12.0	0.0	120	24.5	2.3	0.1	25.14	3	0
1918.00	0.00		1918	120	12.0	0.0	120	25.5	2.2	0.3	23.11	4	0
1954.71	0.02	0.001	1957	119	11.7	0.3	120	144.0	10.4	0.8		3	0
623.13	0.01	0.001	623	116	0.0		59	1.8	0.2	0.0	1.60	4	1
712.25	0.06	0.022	712	116	0.0		59	8.6	0.4	0.1	7.00	5	1
819.61	0.03	0.001	820	116	0.0		59	2.5	0.2	0.0	2.40	5	1

*The subscripts *B*, *ext*, and *endf* refer to final Bayesian uncertainties, external uncertainties, and ENDF resonance parameters, respectively. Resonance spins J were taken from ENDF/B-VIII.0. Parameters for which no errors are listed were not varied by SAMMY. The energies listed in columns 1 through 4 are in units of electron volts (eV) and the energies listed in columns 5 through 12 are in units of milli electron volts (meV).

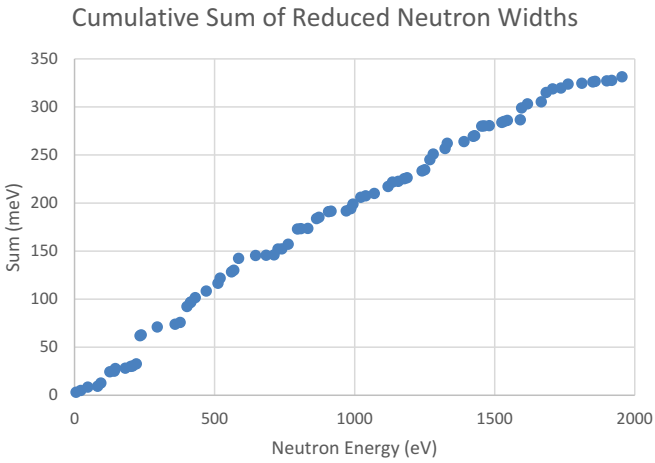

Fig. 8. The cumulative sum of Cs reduced neutron widths for all positive energy s-wave resonances up to 2000 eV.

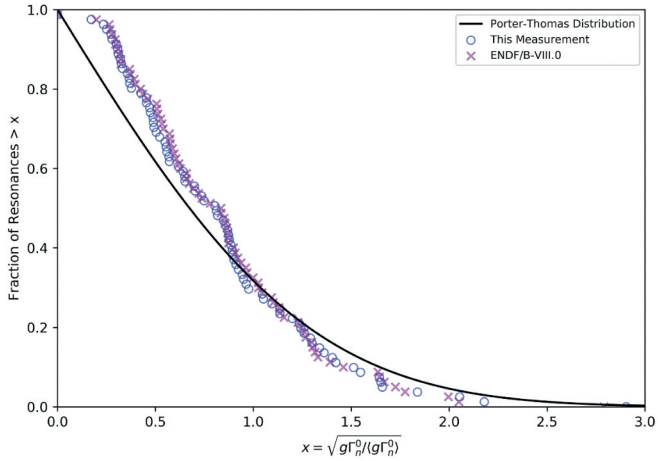

Fig. 9. Cumulative reduced width distributions for ^{133}Cs parameters for this measurement and ENDF parameters. These are plotted along with a Porter-Thomas distribution.

The Cs strength functions for $J = 3$, $J = 4$, and all the resonances are listed in Table V. These strength functions are for resonances below 1800 eV. The errors are based on the $\Delta\Gamma_{n,B}$ values listed in Table IV.

The distribution of reduced neutron widths of s-wave resonances below the neutron energy 2000 eV is plotted in Fig. 9. Figure 9 shows the distribution for the widths determined in this experiment, the ENDF widths, and a Porter-Thomas distribution.[9] The measured and ENDF reduced neutron widths lie above the Porter-Thomas distribution below $x \approx 1$ and below the Porter-Thomas distribution above $x \approx 1$. The measured and ENDF reduced widths are approximately equal to each other above $x \approx 0.5$ whereas the measured reduced widths are slightly smaller than the ENDF values below $x \approx 0.5$.

V. CONCLUSIONS

The combined analysis of capture and transmission measurements in ^{133}Cs has been extended from 600 to 2000 eV. Resonance parameters have been determined for 52 s-wave and 1 p-wave resonances in this energy range. The s-wave strength function for all the resonances in the 0- to 2000-eV neutron energy range is $(1.626 \pm 0.008) \times 10^{-4}$. The reduced neutron width distribution for these resonances in the 0- to 2000-eV neutron energy range is similar to the Porter-Thomas distribution. The correction for false capture in the multiplicity detector now enables this detector to be extended to energies well above 600 eV.

APPENDIX

RATIO OF FALSE CAPTURE TO CAPTURE IN A SINGLE RESONANCE

The ratio of false capture to capture in an isolated resonance is a useful measure of the importance of false capture. The following analysis ignores multiple scattering in the sample and is thus only an approximate measure of false capture.

The capture yield times the differential energy $Y_\gamma(E)$ dE from a sample at neutron energy E is

$$Y_\gamma(E)dE = \left[1 - e^{-N\sigma_t(E)}\right]\frac{\sigma_\gamma(E)}{\sigma_t(E)}dE \ . \qquad \text{(A.1)}$$

The capture yield integrated over the resonance is

TABLE V

Cesium Strength Functions for Spin 3, Spin 4, and All Resonances Combined for s-Wave Resonances Below 1800 eV

$SF_{J=3}$	$SF_{J=4}$	$SF_{all\ resonances}$
$(0.683 \pm 0.004) \times 10^{-4}$	$(0.920 \pm 0.003) \times 10^{-4}$	$(1.626 \pm 0.008) \times 10^{-4}$

$$Y_\gamma(E)dE = \left[1 - e^{-N\sigma_t(E)}\right]\frac{\sigma_\gamma(E)}{\sigma_t(E)}dE \approx \frac{\Gamma_\gamma}{\Gamma}\left[1 - e^{-N\sigma_t(E)}\right]dE \quad , \tag{A.2}$$

where the ratio of cross sections inside the integral has been replaced by the ratio of radiation to total widths outside the integral. This is possible because over the region where the resonance cross section is significant, the approximation is reasonably accurate.

The neutron yield times the differential energy $Y_n(E)dE$ is

$$Y_n(E)dE = \left[1 - e^{-N\sigma_t(E)}\right]\frac{\sigma_n(E)}{\sigma_t(E)}dE \quad . \tag{A.3}$$

The total false capture produced at energy E times the differential energy $Y_{FC,tot}(E)dE$ is

$$Y_{FC,tot}dE = FCSN(E) \times Y_n(E)dE = FCSN(E)\left[1 - e^{-N\sigma_t(E)}\right]\frac{\sigma_n(E)}{\sigma_t(E)}dE \quad , \tag{A.4}$$

where $FCSN(E)$ is the number of false captures produced per scattered neutron per unit energy at neutron energy E. Integrating the total false capture over the resonance yields

$$Y_{FC,tot}dE = FCSN(E)\left[1 - e^{-N\sigma_t(E)}\right]\frac{\sigma_n(E)}{\sigma_t(E)}dE \approx FCSN(E_o)\frac{\Gamma_n}{\Gamma}\left[1 - e^{-N\sigma_t(E)}\right]dE \quad , \tag{A.5}$$

where the ratio of widths outside the integral has been substituted for the ratio of cross sections inside the integral and the number of false captures per scattered neutron has been pulled out of the integral and evaluated at the resonance energy E_o.

To obtain the ratio of false captures in a resonance to captures in a resonance, we divide Eq. (A.5) by Eq. (A.2) to obtain the expression

$$\textit{Ratio of false captures to captures in a resonance} \approx FCSN(E_o)\frac{\Gamma_n}{\Gamma_\gamma}. \tag{A.6}$$

The integrals and total widths have divided out, and we have a simple expression that contains the neutron and radiation widths of the resonance and the number of false captures per scattered neutron evaluated at the resonance energy E_o.

Equation (A.6) was applied to the Cs resonances from 600 to 2000 eV using ENDF resonance widths and the false capture per scattered neutron obtained from the lead scattering measurement (see Sec. III.C and Fig. 3). The largest ratio was 11% for one resonance, and only 16% of the resonances had a ratio greater than 4%.

Acknowledgments

The authors gratefully acknowledge the Gaerttner LINAC Center staff for both operating the accelerator during these measurements and providing the mechanical and electronic assistance needed. This paper has been authored by the Naval Nuclear Laboratory, operated by Fluor Marine Propulsion, LLC, under contract number 89233018CNR000004 with the U.S. Department of Energy.

References

1. R. C. BLOCK et al., "Neutron Transmission and Capture Measurements of ^{133}Cs from 0.01 to 600 eV," *Nucl. Sci. Eng.*, **193**, 269 (2019); https://doi.org/10.1080/00295639.2018.1520526.

2. D. P. BARRY, "Neodymium Neutron Transmission and Capture Measurements and Development of a New Transmission Detector," PhD Thesis, Rensselaer Polytechnic Institute (2003).

3. R. C. BLOCK et al., "A Multiplicity Detector for Accurate Low-Energy Neutron Capture Measurements," *Proc. Int. Conf. Nuclear Data for Science and Technology*, Mito, Japan, May 30–June 3, 1988, p. 383 (1988).

4. Y. DANON et al., "Simultaneous Measurement of ^{235}U Fission and Capture Cross Sections from 0.01 eV to 3 keV Using a Gamma Multiplicity Detector," *Nucl. Sci. Eng.*, **187**, 291 (2017); https://doi.org/10.1080/00295639.2017.1312937.

5. N. M. LARSON, "Updated User's Guide for SAMMY: Multilevel R-Matrix Fits to Neutron Data Using Bayes Equations," ORNL/TM-9179/R8 ENDF-364/R2, Oak Ridge National Laboratory (Oct. 2008).

6. S. A. POZZI, E. PADOVANI, and M. MARSEGUERRA, "MCNP-PoliMi: A Monte-Carlo Code for Correlation Measurements," *Nucl. Instrum. Meth. Phys. Res. A*, **513**, 550 (2003); https://doi.org/10.1016/j.nima.2003.06.012.

7. D. A. BROWN et al., "ENDF/B-VIII.0," *Nucl. Data Sheets*, **148**, 1 (2018); https://doi.org/10.1016/j.nds.2018.02.001.
8. H. I. LIOU and J. RAINWATER, "Uncertainty in the Neutron-Strength-Function Evaluation for a Small Number of Resonances," *Phys. Rev. C*, **6**, 435 (1972); https://doi.org/10.1103/PhysRevC.6.435.
9. C. E. PORTER and R. G. THOMAS, "Fluctuations of Nuclear Reaction Widths," *Phys. Rev.*, **104**, *2*, 483 (1956); https://doi.org/10.1103/PhysRev.104.483.